

Article

Electronic and Molecular Adsorption Properties of Pt-Doped BC₆N: An Ab-Initio Investigation

Nada M. Alghamdi¹, Mohamed M. Fadlallah^{2,*} , Hind M. Al-qahtani³ and Ahmed A. Maarouf^{4,*} 

¹ Department of Physics, College of Science, Imam Abdulrahman Bin Faisal University, Dammam 31441, Saudi Arabia; nmghamdi@iau.edu.sa

² Physics Department, Faculty of Science, Benha University, Benha 13518, Egypt

³ Department of Physics, College of Science and Humanities, Imam Abdulrahman Bin Faisal University, Jubail 35811, Saudi Arabia; halqahtani@iau.edu.sa

⁴ Department of Physics, Faculty of Basic Sciences, German University in Cairo, New Cairo City 11835, Egypt

* Correspondence: mohamed.fadlallah@fsc.bu.edu.eg (M.M.F.); ahmed.maarouf@guc.edu.eg (A.A.M.)

Abstract: In the last two decades, significant efforts have been particularly invested in two-dimensional (2D) hexagonal boron carbon nitride $h\text{-B}_x\text{C}_y\text{N}_z$ because of its unique physical and chemical characteristics. The presence of the carbon atoms lowers the large gap of its cousin structure, boron nitride (BN), making it more suitable for various applications. Here, we use density functional theory to study the structural, electronic, and magnetic properties of Pt-doped BC₆N (Pt-BC₆N, as well as its adsorption potential of small molecular gases (NO, NO₂, CO₂, NH₃). We consider all distinct locations of the Pt atom in the supercell (B, N, and two C sites). Different adsorption locations are also considered for the pristine and Pt-doped systems. The formation energies of all Pt-doped structures are close to those of the pristine system, reflecting their stability. The pristine BC₆N is semiconducting, so doping with Pt at the B and N sites gives a diluted magnetic semiconductor while doping at the C1 and C2 sites results in a smaller gap semiconductor. We find that all doped structures exhibit direct band gaps. The studied molecules are very weakly physisorbed on the pristine structure. Pt doping leads to much stronger interactions, where NO, NO₂, and NH₃ chemisorb on the doped systems, and CO₂ physisorb, illustrating the doped systems' potential for gas purification applications. We also find that the adsorption changes the electronic and magnetic properties of the doped systems, inviting their consideration for spintronics and gas sensing.



Citation: Alghamdi, N.M.; Fadlallah, M.M.; Al-qahtani, H.M.; Maarouf, A.A. Electronic and Molecular

Adsorption Properties of Pt-Doped BC₆N: An Ab-Initio Investigation.

Nanomaterials **2024**, *14*, 762. <https://doi.org/10.3390/nano14090762>

Received: 10 March 2024

Revised: 16 April 2024

Accepted: 20 April 2024

Published: 26 April 2024



Copyright: © 2024 by the authors. Licensee MDPI, Basel, Switzerland. This article is an open access article distributed under the terms and conditions of the Creative Commons Attribution (CC BY) license (<https://creativecommons.org/licenses/by/4.0/>).

Keywords: hexagonal boron nitride; electronic properties; doping; molecular adsorption; ab-initio calculations

1. Introduction

Since graphene's fabrication in 2004 [1], two-dimensional (2D) materials have gained considerable experimental and theoretical interest. The reduced dimensionality of these materials and the wide variety of their structural and compositional properties have promised great technological utilization. This interest is boosted by the progress in experimental and characterization methods, which reflects on the potential of fabricating complex structures with specific physical or chemical properties.

Perhaps the most commonly known 2D material is graphene, which possesses unique electronic, mechanical, and optical properties that nominate it for many technological applications [2]. However, some shortcomings in graphene, like its lack of an electronic band gap, led researchers to look for other graphene-like materials [3,4]. Silicene [5], germanene [6], hexagonal boron nitride (h-BN) [7], transition metal dichalcogenides (TMDs) [3,8], MXenes [9,10], and Mo(W)Si₂N₄ [11] are examples of 2D materials that mostly have a honeycomb structure, associated with some great features not existing in 3D materials, such as large surface area, high optical transparency, and active sites. The special physical and chemical properties exhibited by 2D materials make them excellent candidates for many

potential applications, such as photocatalysis [12], field-effect transistors [13], hydrogen storage [14,15], and gas sensing [16–18].

Boron, nitrogen, and carbon are contemporaries on the periodic table. Carbon forms strong covalent bonds with boron and nitrogen, while boron and nitrogen form covalent-polarized bonds. This leads to a variety of (h - $B_xC_yN_z$) compounds [19,20] that recently gained much interest [21]. The replacement of B or N by C may offer a way to tune the properties of those systems without causing any significant lattice distortion. Introducing BN patches into the graphene lattice has been shown to change it from a semimetal to a semiconductor. The Dirac point disappears, and a direct band gap opens at the K points [22–24]. It is thus expected that changing the relative compositions of B, C, and N in h - $B_xC_yN_z$ structures may lead to a rich spectrum of physical properties.

Several ternary B-C-N molecule compositions (for example, BCN, BC_2N , BC_4N , BC_6N , and B_2CN) have been fabricated utilizing a variety of methodologies such as chemical vapor coating, a solvothermal approach, and a chemical reaction approach [25]. BC_2N also captured the attention of researchers since it is expected to be more thermally stable and chemically inert than diamond and harder than c -BN [22,26]. BCN has a wide range of applications, such as oxidation of contaminants and colorants, hydrogen production from water, clear photovoltaic cell fabrication, UV absorption, optoelectronics, fire-resistant materials, and catalysis for a wide range of chemical interactions [27,28].

Recently, BC_6N 2D quantum dots have been successfully synthesized by doping graphene quantum dots with boron and nitrogen atoms [29]. The material is found to be a semiconductor with a band gap of 1.2–1.3 eV [30,31]. Because of the graphene-like structure of BC_6N , it shares some of graphene's physical and mechanical properties, such as high stiffness and high thermal conductivity [19,31]. Numerous studies have been conducted on BC_6N to tailor its properties for various applications. It is possible to induce metallic, half-metallic, or dilute magnetic semiconductor behavior by substitutional and adsorption doping in BC_6N [30,31]. Furthermore, defects such as vacancies alter the electrostatic landscape of BC_6N , making it sensitive to specific gases [30,31].

With their high intrinsic activity, noble metals can modify the electronic structure of 2D materials and enhance the interaction between gases and nanomaterials. Thus, researchers are becoming more and more interested in noble metal dopings. For example, Pt-doped 2D $MoSe_2$ [32,33] can be an efficient electrocatalyst for both hydrogen evolution and oxygen reduction reactions. Pt dopant improves the absorption of 2D $Ti_3C_2T_2$ Mxene for SF_6 [34]. CO, NO, NO_2 , O_2 , and NH_3 molecules can chemisorb on a Pt-doped arsenene sheet [35].

Although pristine BC_6N has been studied, structures doped with various elements must be investigated. Here, we use spin-polarized density functional theory to analyze the electronic and molecular adsorption properties of Pt-doped BC_6N . We consider a 3×3 supercell of BC_6N (72 atoms) and study the substitutional Pt-doping of these systems. This supercell allows for a reasonable and experimentally common doping percentage of Pt ($\sim 1\%$) and minimizes the interaction between adsorbed molecules in neighboring cells, thereby giving a more accurate estimate of the adsorption energies. The supercell has four symmetrically inequivalent sites: B, N, and two C atoms (C1 and C2). We perform the structural relaxation and calculate the densities of states of each system. We then study the adsorption of four gases (NO, CO_2 , NO_2 , and NH_3) on each system, determining their adsorption energies, as well as their effect on the electronic properties of the doped- BC_6N nanosheets.

2. Computational Methods

We used first-principle calculations based on spin-polarized density functional theory (DFT) as implemented in the Quantum Espresso (QE) plane waves package [36] V6.5 widely used to study the physical properties of periodic systems. The exchange–correlation interaction is described by the generalized gradient approximation (GGA) via the Perdew–Burke–Ernzerhof (PBE) functional [37], and with ultrasoft pseudopotentials (rrkjus-psl version of the QE pseudopotential PS library). An energy cut-off of 55 Ry for the wavefunc-

tion, and 550 Ry for the charge density are utilized for all SCF calculations. Our base system is a 3×3 supercell of BC_6N , with a total of $n = 72$ atoms. Doped systems are constructed by substituting a dopant atom for B, N, or C (2 positions). A vacuum spacing of 20 Å avoids any interaction between neighboring images. All systems are fully relaxed (volume and ionic positions) until the forces on the atoms become less than 0.001 Ry/Bohr. Van der Waals interactions (vdW-DF) [38] are included in our study. Brillouin zone integrations are performed using the tetrahedron method and a $12 \times 12 \times 1$ k -point grid to calculate the density of states (DOS). Band structures are calculated with 80 k -points along the path $\Gamma\text{MK}\Gamma$. Charge transfer from/to the BC_6N systems is determined by calculating the Löwdin charges. The formation energy E_f per atom is calculated to check the structural stability of different Pt- BC_6N systems

$$E_f = (E(\text{Pt} - \text{BC}_6\text{N}) + E(X) - E(\text{BC}_6\text{N}) - E(\text{Pt}))/n, \quad (1)$$

where $E(\text{Pt} - \text{BC}_6\text{N})$, $E(X)$, $E(\text{BC}_6\text{N})$, and $E(\text{Pt})$ are the energies of the doped sheet, isolated native atom (B, N, C1 or C2), pristine sheet, and isolated Pt atom in the same supercell, respectively. The adsorption energy is evaluated by

$$E_{ad} = E(\text{sheet}) + E(\text{molecule}) - E(\text{sheet} + \text{molecule}). \quad (2)$$

where $E(\text{sheet} + \text{molecule})$, $E(\text{sheet})$, and $E(\text{molecule})$ are the energies of the sheet or doped sheet with the adsorbed molecule, sheet or doped sheet without the adsorbed molecule, and the isolated molecule in the same supercell volume, respectively.

3. Results

BC_6N has a unit cell composed of 6 C atoms, 1 B, and 1 N atoms. The 6 C positions include two distinct sites: a C atom with a B or an N nearest neighbors. In order to study doping with regular experimental percentages, we construct a 3×3 supercell of BC_6N with a total of 72 atoms. To establish a reference, we begin by calculating the electronic properties of this pristine system. The optimized atomic structure of a hexagonal BC_6N is shown in Figure 1a. Our calculated bond lengths are: C-C = 1.41 Å, C-B = 1.47 Å, and C-N = 1.46 Å, which is in agreement with previous work [30,31,39,40].

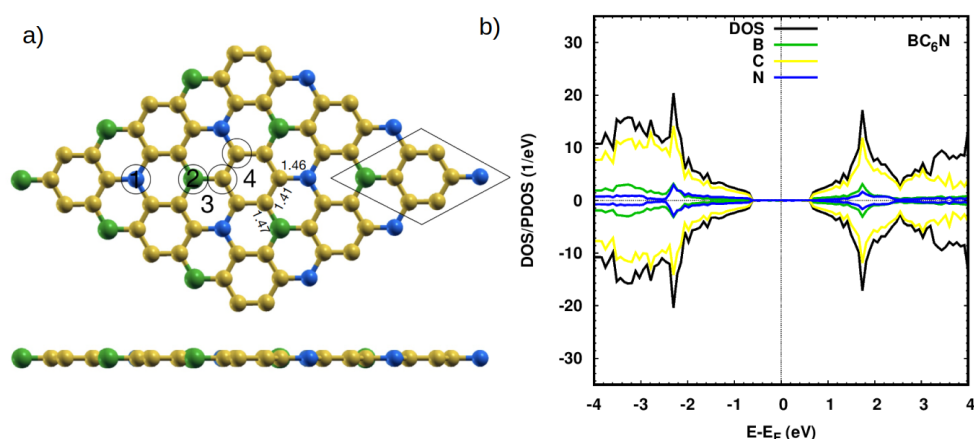


Figure 1. (a) Top and side view of the optimized atomic structure of a pristine hexagonal 3×3 supercell of a BC_6N sheet. The black parallelogram marks the original unit cell of BC_6N . Yellow, green, and blue spheres represent C, B, and N atoms, respectively. Bond lengths are given in Å. The numbers “1” (top on N (TN)), “2” (top on B (TB)), “3” (top on BNC hexagonal (H1)), and “4” (top on C hexagonal (H2)) indicate the adsorption sites of gases on the BC_6N , whereas the circles refer to the doping sites where the systems are doped with a Pt atom. (b) Projected DOS (PDOS) of the pristine BC_6N system showing the most significant contributions.

Figure 1b shows the projected density of states of the pristine system. The system is semiconducting with a bandgap of 1.3 eV, which matches previous work [30,31,39,40]. The main contributions to the valence and conduction bands are due to the C states, with a small contribution from the N(B) states—the second dominant species in the valence (conduction) band. The bandgap of BC₆N means that it can be a promising material for optoelectronic applications. The Löwdin charge analysis shows that C1 and N gain electronic charge, while C2 and B lose some charge, consistent with the electronegativities of those atoms and their neighbors.

We now begin to dope our systems. A look at the BC₆N original unit cell (black parallelogram, Figure 1a shows that there are four distinct locations. Two locations are at the B and N atoms, and the other two are the sites of the C atoms in black circles. The two carbon sites are inequivalent. One site (C1) is connected to two carbon atoms and one boron atom, while the other (C2) is connected to two carbon atoms and one nitrogen site.

3.1. Pt-Doping

The relaxed structures of the Pt-doped systems are shown in Figure 2a–d. Minimum deformation in the vicinity of the Pt atom occurs with the Pt at the B site (Pt_B), the C1 site (Pt_{C1}), and the C2 site (Pt_{C2}), (Figure 2a–c), and the Pt atom is the out-of-plane bulge of about 1.80 Å with bond lengths (with the nearby atoms) of 1.97 Å, 2.08 Å, 1.96 Å, respectively. The bond length of Pt_{C2} is large due to the atomic size of the B atom as compared to the C and N atoms. The other case is Pt instead of N (Pt_N), which exhibits an out-of-plane bulge of about 1.6 Å and bond length of 1.97 Å (Figure 2d). The vertical deformation can be understood with the help of the system's Löwdin charge analysis. For the Pt_N doped system, the charge difference ΔQ on the Pt atom and its three nearest neighbors is $+0.39e$, $-0.17e$, $-0.167e$ and $-0.168e$. The corresponding distribution of the Pt_{C2} doped system is $+0.43e$, $-0.15e$, $-0.042e$, and $-0.005e$. The bulge around the Pt atom is caused by the difference between the Pt charge and the charges of the neighboring atoms cause the bulge. A much smaller out-of-plane deformation is seen for the Pt_B-doped system, with $+0.08e$, $+0.05e$, $+0.06e$ and $+0.07e$, and for the Pt_{C1}-doped system, with $+0.1e$, $-0.08e$, $-0.1e$ and $-0.16e$. The formation energy calculations (Equation (1)) indicate the Pt_N-BC₆N has a slightly lower energy (0.05 eV) as compared to the other doped structures, which have the same formation energy per atom (0.09 eV), Table 1.

The DOS spectrum of the Pt_B-BC₆N is spin asymmetric (Figure 2e), especially in the conduction band, which sees significant contributions from the Pt states (such as at 0.2 eV and 0.4 eV) and the C states. The valence band continues to be dominated by the C states. The band gap of the spin-down spectrum is similar to that of the pristine system (1.3 eV), while the spin-up gap becomes 0.2 eV due to the occupation of states localized on the Pt atom and its three nearest carbon neighbors. The asymmetric behavior of the two spin components indicates the structure is magnetic with 0.9 μ_B , and hence, the structure is a diluted magnetic semiconductor (DMSC). For Pt_{C1}- and Pt_{C2}-BC₆N, the DOS of the two spin channels is symmetric, so the structure is non-magnetic. Due to the contribution of Pt states, as in the valence band, the band gaps decrease to 1.1 eV and 0.5 eV, compared to pristine BC₆N. The last substitutional doping is Pt_N. The Fermi energy is shifted to the conduction band, and the structure is a diluted semiconductor with a spin-up and spin-down band gap of 0.2 eV and 1.4 eV, respectively. The asymmetric behavior of the DOS for two spin components in the conduction band gives the structure a magnetization of 1 μ_B . All band gaps are direct ones, as is clear from the band structures of the Pt-doped systems (Figure 2i–l).

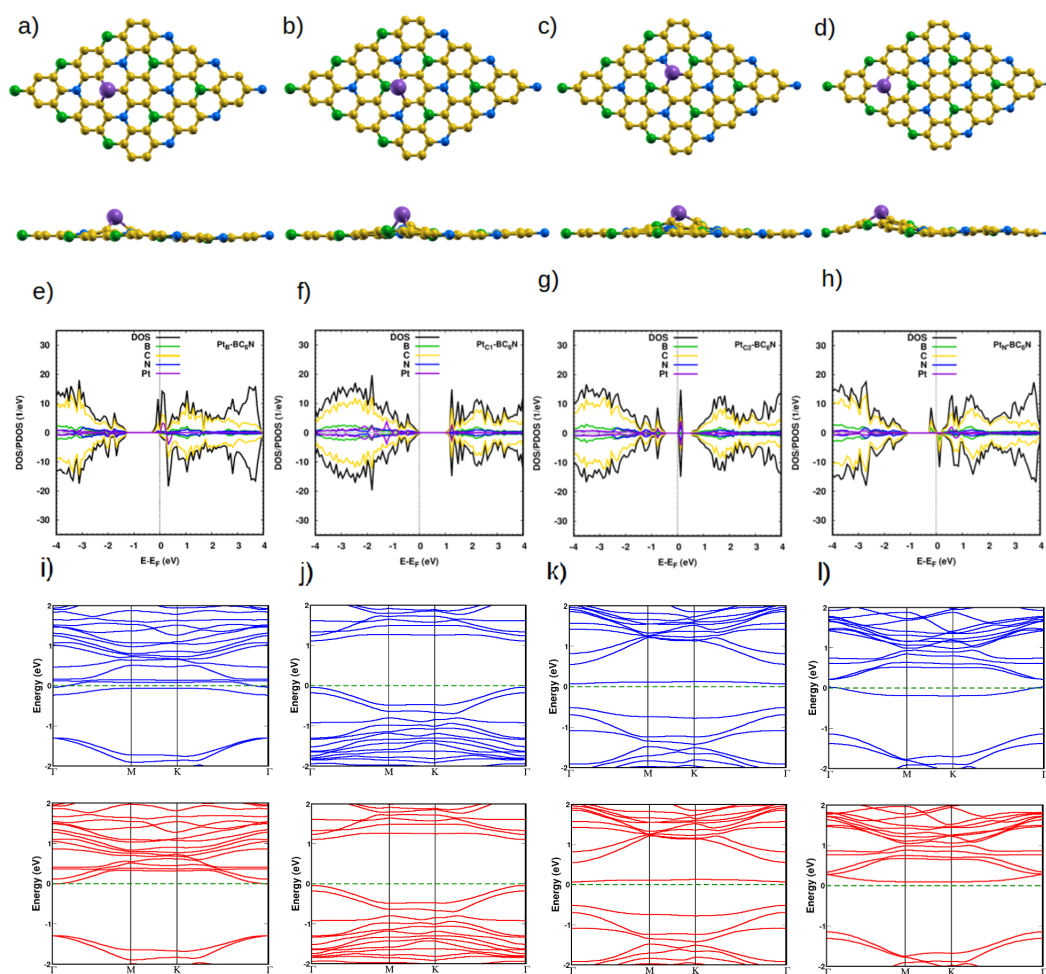


Figure 2. (a–d) Top and side view of the optimized atomic structure of Pt-BC₆N sheet with different doping sites, Pt_B, Pt_{C1}, Pt_{C2}, and Pt_N, respectively. The purple sphere represents the Pt atom. (e–h) The corresponding DOS/projected DOS (PDOS) of the Pt-BC₆N system shows the most significant contributions. (i–l) The corresponding band structure, from –2 eV to 2 eV. Spin-up (down) is in blue (red).

Table 1. Pt-BC₆N: the charge transfer (ΔQ (*e*)), formation energy (E_f (meV)), magnetization (Mag (μ_B)), band gap (E_g (eV)).

Systems	ΔQ	E_f	Mag	E_g (up)	E_g (dn)
BC ₆ N	-	-	0.0	1.3	1.3
Pt _B -BC ₆ N	0.08	87	0.9	0.2	1.3
Pt _{C1} -BC ₆ N	0.10	88	0.0	1.1	1.1
Pt _{C2} -BC ₆ N	0.43	94	0.0	0.5	0.5
Pt _N -BC ₆ N	0.39	51	1.0	0.2	1.4

3.2. Molecules Adsorption on Pristine and Pt-Doped BC₆N Systems

We now discuss the molecular adsorption properties of our systems. We consider four gas molecules, NO, NO₂, CO₂, and NH₃. Each molecule is initially placed above each of the distinct sites (TB (@_{TB}), TN (@_{TN}), H1 (@_{H1}), and H2 (@_{H2})) for pristine BC₆N, and (Pt_B, Pt_{C1}, Pt_{C2}, and Pt_N) for the doped Pt-BC₆N sheet, and then the system is structurally relaxed. The relaxation starts from a high symmetry orientation of the molecule so that we allow it to choose the atom it faces the sheet with. We then calculate the system's various

electronic parameters. We will include the adsorption results on pristine structures to form a reference for comparison.

3.2.1. Adsorption of NO

The molecular N-O bond length is 1.16 Å, which agrees well with previous calculations [9]. When NO is placed on the pristine sheet above any position, there is no significant change in its bond length. We find the distances between the N atom and the nearest atoms of our 4 sheets are 2.83 Å, 3.10 Å, 3.10 Å, and 2.88 Å, and with adsorption energies of 0.15 eV, 0.14 eV, 0.12 eV, and 0.17 eV, for the TB, TN, H1, and H2 positions, respectively (Table 2). The NO molecules adsorb very weakly ($E_{ad} < 0.2$ eV) on the pristine structure at all adsorption sites (Table 2), leading to negligible effects on the DOS of the pristine system (Figure 3). As expected, no significant charge transfer occurs (Table 2).

Table 2. NO adsorption NO pristine and Pt-BC₆N: the closest distance (d (Å)), nearest atom (X), charge transfer (ΔQ (e)), adsorption energy (E_{ad} (eV)), magnetization (Mag (μ_B)), band gap (E_g (eV)).

Systems	d	X	ΔQ	E_{ad}	Mag	E_g (up)	E_g (dn)
@ _{TB} BC ₆ N	2.8	N	−0.04	0.2	1.0	0.4	1.1
@ _{TN} BC ₆ N	3.1	N	0.00	0.1	1.0	1.1	0.4
@ _{H1} BC ₆ N	3.1	N	−0.04	0.1	1.0	0.3	1.2
@ _{H2} BC ₆ N	2.9	N	−0.05	0.2	1.0	0.5	1.3
@Pt _B -BC ₆ N	1.9	N	−0.20	2.7	2.1	1.1	0.8
@Pt _{C1} -BC ₆ N	1.9	N	−0.21	2.3	1.0	0.9	0.9
@Pt _{C2} -BC ₆ N	1.9	N	−0.15	2.3	0.7	0.2	-
@Pt _N -BC ₆ N	2.0	N	−0.20	2.1	2.1	1.2	0.9

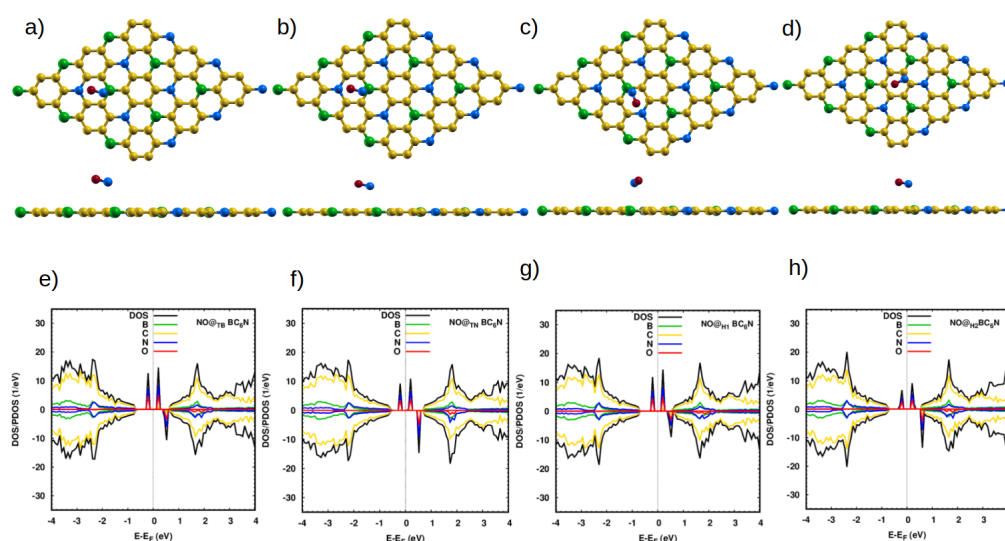


Figure 3. Top and side view of the optimized atomic structure of NO@BC₆N sheet with different doping sites: (a) NO@_{TB}BC₆N, (b) NO@_{TN}BC₆N, (c) NO@_{H1}BC₆N and (d) NO@_{H2}BC₆N. (e–h) The corresponding DOS/Projected DOS (PDOS) of the NO@BC₆N systems. The red spheres represent O atoms.

The situation is very different with the Pt-doped system. The closest distances between the N atom of the molecule and the Pt dopant atom are 1.93 Å, 1.90 Å, 1.87 Å, and 1.98 Å for NO@Pt_{TB}-, NO@Pt_{TN}-, NO@Pt_{C1}-, and NO@Pt_{C2}-BC₆N, respectively. These are much smaller than the corresponding distances for the pristine system, indicating the much stronger interaction between the NO molecule and the doped sheet. Furthermore, the bond length of N-O increases to 1.198 Å for NO@Pt_{TB}, NO@Pt_N and 1.2 Å for NO@Pt_{C1}, NO@Pt_{C2}. The adsorption energies are significantly higher: 2.65 eV, 2.27 eV, 2.27 eV, and 2.06 eV for Pt_B-, Pt_{C1}-, Pt_{C2}-, and Pt_N-BC₆N sheets.

Figure 4e shows the DOS/PDOS of NO@Pt_B-BC₆N. The top of the valence band is disturbed by the N and O states, such as for the spin-up component. Also, the mid-gap states are created at 0.4 eV by the N, O, and C states. The band gap becomes 1.1 eV (0.8 eV) for the spin-up (spin-down) component. The structure is a DMSC as Pt_B-BC₆N, with a magnetic moment of 2 μ_B .

For adsorption atop the Pt at the C1 site, the valence and conduction bands of the structure are disturbed asymmetrically for the two spin components, leading to a DMSC with a magnetic moment of 1 μ_B (Figure 4f). The band gap of the spin-up/down component is 0.9 eV. The Pt_{C2}-BC₆N structure (Figure 4g) is a half metal, with a spin-down band gap of 0.2 eV and magnetic moment of 1 μ_B , which can be utilized for spintronic applications. Finally, adsorption on the Pt_N-BC₆N system exhibits the highest structural deformation at the Pt_N site (Figure 4h), leading to a higher effect on the DOS compared to adsorption at other locations. The system has a magnetization of 2 μ_B and spin-up/down gaps of 1.2 eV/0.9 eV. Charge analysis and charge density maps (Figure 4i–l) indicate that charge is transferred from the sheet to the NO molecule, causing the polarization of the N atom of the gas to decrease, and that of the O atom to increase.

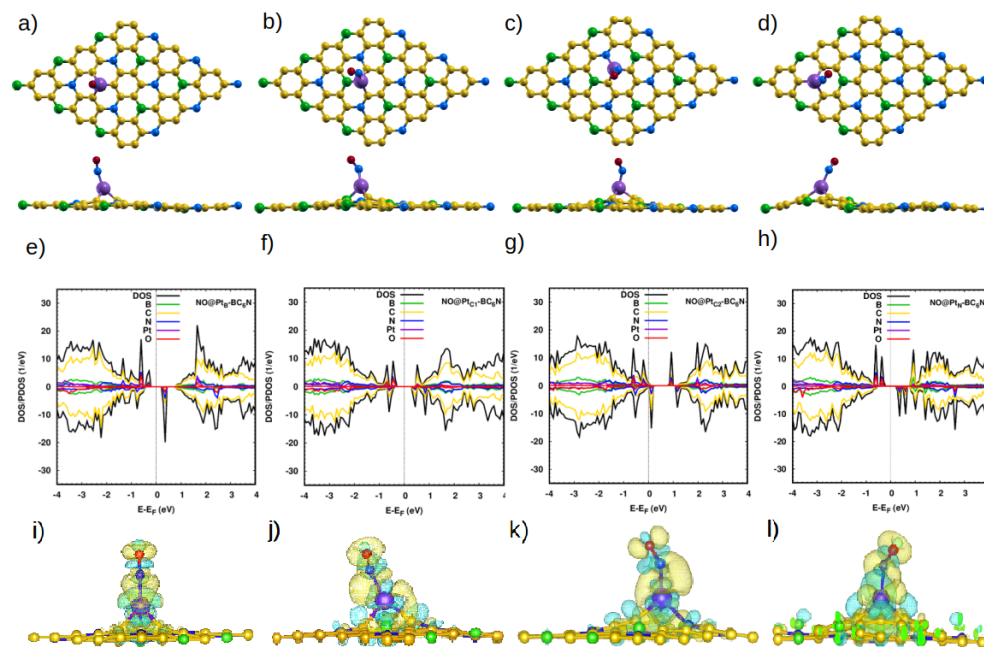


Figure 4. (a–d) Top and side view of the optimized atomic structure of NO@Pt-BC₆N sheet with different doping sites: (a) NO@Pt_B-BC₆N, (b) NO@Pt_{C1}-BC₆N, (c) NO@Pt_{C2}-BC₆N, and (d) NO@Pt_N-BC₆N. (e–h) The corresponding DOS/projected DOS (PDOS) and (i–l) the corresponding charge densities of the NO@Pt-BC₆N systems. Isosurface yellow (blue) color represents higher (lower) charge density.

3.2.2. Adsorption of NO₂

We now discuss our NO₂ adsorption results (Figure 5). For the isolated molecule, the N-O bond length and the O-N-O angle are 1.21 Å and 134° [9]. Adsorption on the pristine sheet slightly changes the structure of the molecule; the bond length and the angle slightly change to 1.23 Å and 127° for adsorption on TB, TN, and H1, while the bond angle is about 128.6° for the H2 position. The molecule is very weakly adsorbed at all sites (0.1 eV), and it faces the sheet with an O atom at a distance of ~2.92 Å for the TB, TN, and H1 sites (Table 3). At the H2 site, it is a bit closer (2.8 Å), with its N atom facing the sheet. A small amount of charge is transferred from the sheet to the molecule. Because of the weak adsorption of NO₂ on the pristine system, its effect on the electronic properties of the sheet is minimal, but for the sake of completion, those results are reported in the Supplementary Information (Figure S1).

Table 3. NO₂ adsorption on pristine and PtBC₆N: the closest distance (d (Å)), O-N-O angle (θ°), nearest atom (X), charge transfer (ΔQ (e)), adsorption energy (E_{ad} (eV)), magnetization (Mag (μ_B)), and band gap (E_g (up) and down (dn) (eV)).

Systems	d	θ°	X	ΔQ	E_{ad}	Mag	E_g (up)	E_g (dn)
@ _{TB} BC ₆ N	2.9	126.7	O	−0.07	0.1	0.9	1.4	−
@ _{TN} BC ₆ N	3.0	126.9	O	−0.16	0.1	0.9	1.4	−
@ _{H1} BC ₆ N	3.0	126.9	O	−0.08	0.1	−0.9	−	1.3
@ _{H2} BC ₆ N	2.8	128.6	N	−0.11	0.1	0.9	0.3	1.3
@Pt _B -BC ₆ N	2.0	112.3	O	−0.43	3.0	0.0	1.3	1.3
@Pt _{C1} -BC ₆ N	2.1	123.3	N	−0.34	2.5	0.2	−	−
@Pt _{C2} -BC ₆ N	2.0	124.8	N	−0.30	2.5	0.0	−	−
@Pt _N -BC ₆ N	2.3	111.8	O	−0.41	3.3	0.0	1.2	1.2

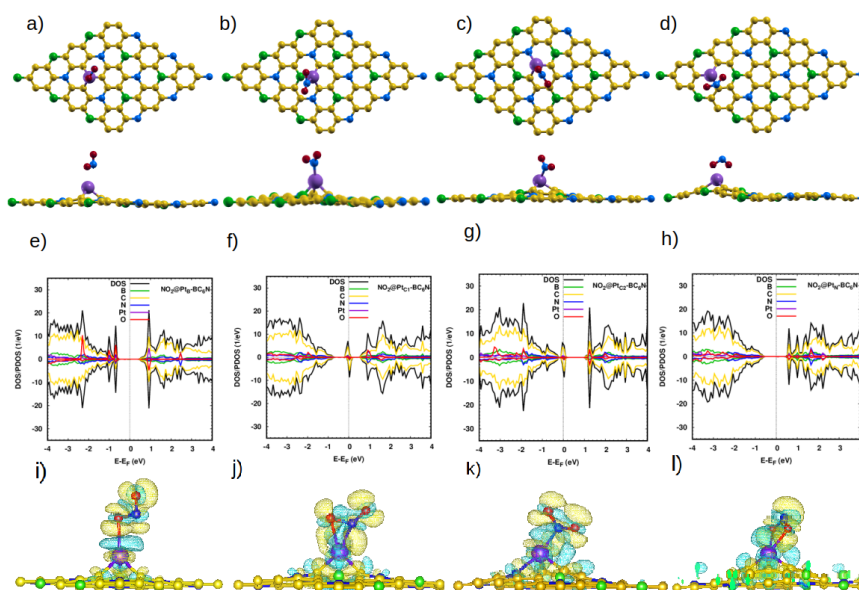


Figure 5. (a–d) Top and side view of the optimized atomic structure of NO₂@Pt-BC₆N sheet with different doping sites: (a) NO₂@Pt_B-BC₆N, (b) NO₂@Pt_{C1}-BC₆N, (c) NO₂@Pt_{C2}-BC₆N, and (d) NO₂@Pt_N-BC₆N. (e–h) The corresponding DOS/projected DOS (PDOS) and (i–l) the corresponding charge densities of the NO₂@Pt-BC₆N systems. Isosurface yellow (blue) color represents higher (lower) charge density.

We now discuss our results for the adsorption of NO₂ on the Pt-doped nanosheets. The N-O bond length is ~ 1.21 Å for all systems. However, the O-N-O angle decreases to 112.3°, 123.3°, 124.8° and 111.8° for Pt_B-, Pt_{C1}-, Pt_{C2}- and Pt_N-BC₆N, respectively. The change in the angle, such as for the cases of NO₂@Pt_B- and NO₂@Pt_N-BC₆N reflects the strong interaction between the nitrogen dioxide molecule and the doped sheet. This is further confirmed by the shorter distance between the molecule and the Pt atom, as well as the charge transfer between the molecule and the sheets ($\sim 0.35e$, Table 3). The charge density maps (Figure 5i–l) show the distribution of the transferred charge around the NO₂ molecule. Therefore, the adsorption of NO₂ is improved by Pt doping. As expected, the NO₂@Pt_B- and NO₂@Pt_N-BC₆N have higher adsorption energy as compared to the other positions in the doped monolayer because of the maximal charge localization occurring at the B and N sites.

In Figure 5e–h, we show the effect of NO₂ on the electronic properties of the sheets. Adsorption changes the state and the magnetic moment of Pt-BC₆N, from DMSC to SC, for NO₂@Pt_N with a band gap of 1.3 eV, from SC to metal for NO₂@Pt_{C1} and NO₂@Pt_{C2}-BC₆N, and from DMSC to SC with a band gap of 1.23 eV for NO₂@Pt_B-BC₆N. All the NO₂@Pt-BC₆N monolayers are nonmagnetic, except NO₂@Pt_{C1}-BC₆N, which shows a small magnetization (0.2 μ_B).

3.2.3. Adsorption of CO₂

CO₂ is the second triatomic molecule that we studied. At all considered locations, the average bond length and the O-C-O angle are nearly unchanged (1.17 Å, 179.3° [9]). The interaction with the sheet is weak (0.2 eV, see Table 4 and Figure S2, SI), which is reflected in the equilibrium distance from the sheet (~3.2 Å), and the negligible charge transfer with the sheet (Table 4).

The picture with the Pt-doped system is quite different. The doped sheet adsorbs the CO₂ molecule at a distance of ~2.2 Å, and the O-C-O angle decreases significantly. The electronic structures of CO₂@Pt_B- and CO₂@Pt_N-BC₆N are very similar. They are DMSCs with a magnetic moment of 1.0 μ_B (Figure 6e,h), and with spin-up (down) band gaps of 1.0 eV (0.8 eV), and 1.0 eV (0.9 eV), for CO₂@Pt_B- and CO₂@Pt_N-BC₆N, respectively. On the other hand, CO₂@Pt_{C1}- and Pt_{C2}-BC₆N are non-magnetic semiconductors, with a band gap of 1.1 eV and 0.4 eV, respectively, for both spin directions (Figure 6f,g). The charge transfer from the sheet to the molecule is higher than with the pristine system, and its distribution is shown in Figure 6i–l.

Table 4. CO₂ adsorption on pristine and Pt-BC₆N: The closest distance (d (Å)), O-C-O angle (θ°), nearest atom (X), charge transfer (ΔQ (e)), adsorption energy (E_{ad} (eV)), magnetization (Mag (μ_B)), and band gap (E_g (up) and down (dn) (eV)).

Systems	d	θ°	X	ΔQ	E_{ad}	Mag	E_g (up)	E_g (dn)
@ _{TB} BC ₆ N	3.3	179.3	C	−0.02	0.2	0.0	1.3	1.3
@ _{TN} BC ₆ N	3.2	179.8	C	−0.01	0.2	0.0	1.3	1.3
@ _{H1} BC ₆ N	3.2	179.3	C	−0.02	0.2	0.0	1.3	1.3
@ _{H2} BC ₆ N	3.2	179.3	C	−0.02	0.2	0.0	1.3	1.3
@Pt _B -BC ₆ N	2.2	144.0	C	−0.38	0.7	1.0	1.0	0.8
@Pt _{C1} -BC ₆ N	2.1	141.5	C	−0.42	0.8	0.0	1.1	1.1
@Pt _{C2} -BC ₆ N	2.1	141.0	C	−0.42	0.6	0.0	0.4	0.4
@Pt _N -BC ₆ N	2.2	146.4	C	−0.33	0.4	1.0	1.0	0.9

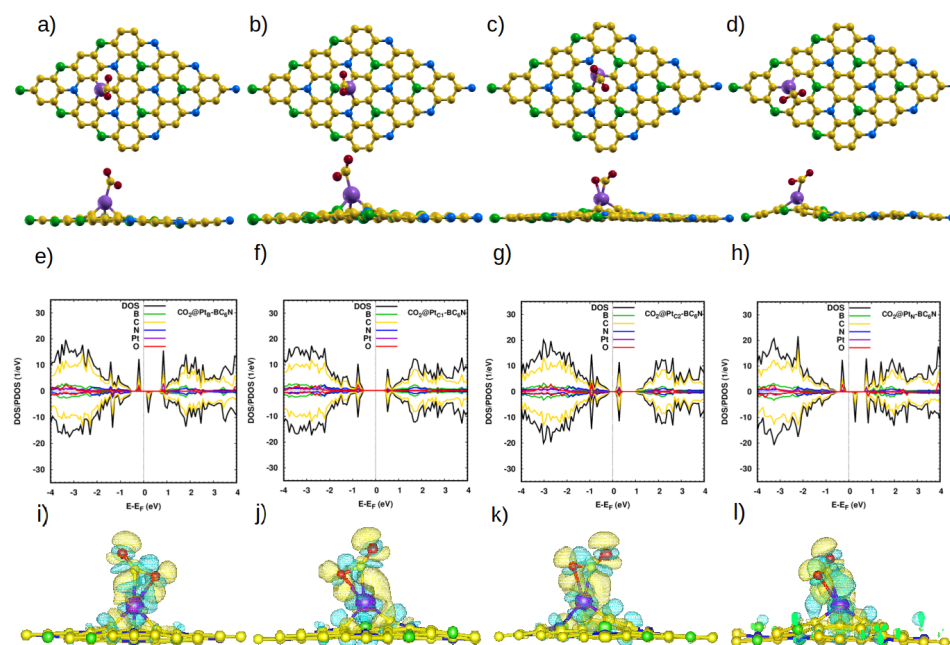


Figure 6. (a–d) Top and side view of the optimized atomic structure of CO₂@Pt-BC₆N sheet with different doping sites: (a) CO₂@Pt_B-BC₆N, (b) CO₂@Pt_{C1}-BC₆N, (c) CO₂@Pt_{C2}-BC₆N, and (d) CO₂@Pt_N-BC₆N. (e–h) The corresponding DOS/projected DOS (PDOS) of the CO₂@Pt-BC₆N systems. (i–l) The corresponding charge density. Isosurface yellow (blue) color represents higher (lower) charge density.

3.2.4. Adsorption of NH₃

The last molecule in our study is NH₃. On the pristine system, the bond length and H-N-H angle of the molecule (1.02 Å and 106.67° [9]) do not change, except for NH₃@_{TB}BC₆N, where the angle is 102.2° (Figure S3). The optimized distance between the closest H atom of the molecule and the sheet is 2.7 Å (Table 5). There is very little charge transfer (<0.1e). Those values reflect the weakness of the interaction between the molecule and the pristine sheet. Indeed, we calculate an adsorption energy of ~0.2 eV.

As with the other studied molecules, the Pt-doped system greatly enhances the adsorption of NH₃ (Table 5). Also, the electronic properties become those of a DMSC with a spin-up (down) band gap of 1.3 eV (0.2 eV) for NH₃@_{TB}-BC₆N (Figure 7e–h). NH₃@_{C1}-BC₆N and NH₃@_{C2}-BC₆N are semiconductors with spin-up (down) band gaps of 1.1 eV and 0.7 eV. Finally, NH₃@_N-BC₆N is a half-metal. Our charge analysis indicates that, contrary to three previous molecules, NH₃ loses charge to the sheet in the four configurations. This is also illustrated in the charge density maps of Figure 7i–l.

Table 5. NH₃ adsorption on pristine and Pt-BC₆N: the closest distance (*d* (Å)), H-N-H angle (θ°), nearest atom (X), charge transfer (ΔQ (e)), adsorption energy (E_{ad} (eV)), magnetization (Mag (μ_B)), and band gap (E_g (up) and down (dn) (eV)).

Systems	<i>d</i>	θ°	X	ΔQ	E_{ad}	Mag	E_g (up)	E_g (dn)
@ _{TB} BC ₆ N	2.7	102.2	H	−0.01	0.2	0.0	1.3	1.3
@ _{TN} BC ₆ N	2.7	106.4	H	−0.01	0.2	0.0	1.3	1.3
@ _{H1} BC ₆ N	2.7	106.2	H	−0.01	0.2	0.0	1.3	1.3
@ _{H2} BC ₆ N	2.8	106.2	H	−0.01	0.2	0.0	1.3	1.3
@ _{TB} -BC ₆ N	2.2	107.3	N	0.22	1.5	−0.9	1.3	0.2
@ _{C1} -BC ₆ N	2.2	107.1	N	0.23	1.6	0.0	1.1	1.1
@ _{C2} -BC ₆ N	2.3	107.3	N	0.21	1.3	0.0	0.7	0.7
@ _N -BC ₆ N	2.3	106.9	N	0.22	1.2	0.9	−	1.4

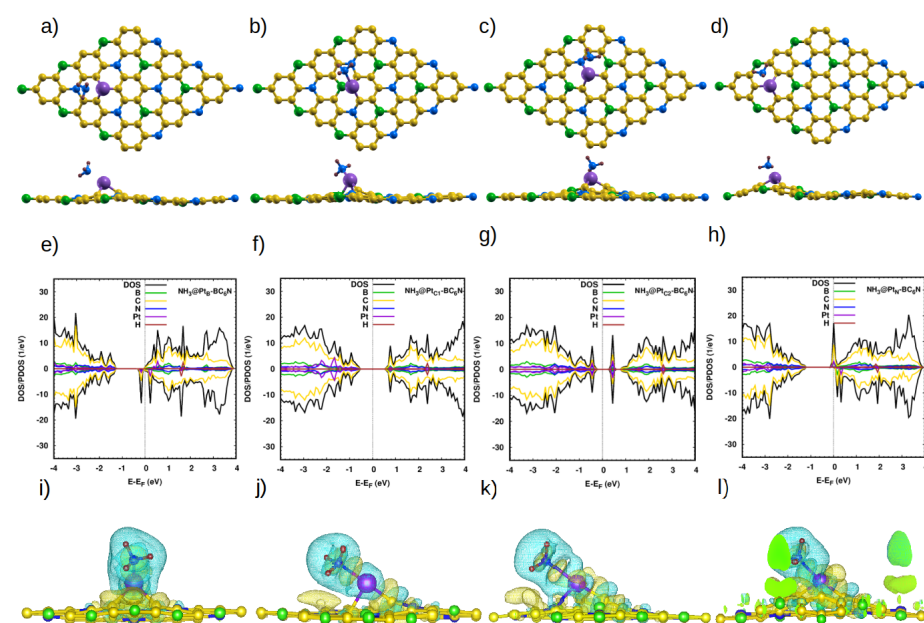


Figure 7. (a–d) Top and side view of the optimized atomic structure of NH₃@Pt-BC₆N sheet with different doping sites: (a) NH₃@_{TB}-BC₆N, (b) NH₃@_{C1}-BC₆N, (c) NH₃@_{C2}-BC₆N, and (d) NH₃@_N-BC₆N. (e–h) The corresponding DOS/projected DOS (PDOS) and (i–l) the corresponding charge densities of the NH₃@Pt-BC₆N systems. Isosurface yellow (blue) color represents higher (lower) charge density. In (l), the isosurface extends to the supercell border, and the green color indicates the interior of the isosurface.

Previous research has demonstrated that Pt-doped 2D materials indeed enhance molecular adsorption and sensing [41]. For example, CO and NO are found to chemisorb on Pt-doped MoS₂ monolayers with adsorption energies of 1.38 eV and 1.21 eV, respectively [42]. Pt-doped monolayer WSe₂ is shown to be suitable for the adsorption of CO₂, NO₂, and SO₂ [43]. A monolayer of Pt-doped HfSe₂ exhibits desirable adsorption behavior for SO₂ and SOF₂ [44]. Our results discussed are in line with previous findings. Computing the average adsorption energy of each gas on the different adsorption sites, one can assess the potential of the Pt-doped BC₆N for gas filtration. As shown in Table 6, NO₂, NO, and NH₃ are chemisorbed on the Pt-doped systems, while CO₂ is physisorbed. This suggests that our Pt-doped systems are suitable for the filtration of NO₂, NO, and NH₃, and to a lesser degree for CO₂. We have also seen that the adsorption of NO₂, NO, NH₃, and CO₂ leads to some changes in the band gaps of our Pt-doped systems, which may be utilized to develop sensors for those gases. Therefore, the Pt-doped BC₆N systems studied in this work are good candidate materials for the filtration/sensing of NO₂, NO, NH₃, and CO₂.

Table 6. Average adsorption energies (E_{ad}^{ave} (eV)) on the Pt-doped systems. The average is taken over the 4 different adsorption sites in each system.

Gas	E_{ad}^{ave}
NO ₂	2.8
NO	2.4
NH ₃	1.4
CO ₂	0.6

4. Conclusions

In this work, we use first principle calculations to investigate the structural, electronic, and magnetic properties of Pt-doped BC₆N (Pt-BC₆N). We also study the adsorption of four common gas molecules (NO, NO₂, CO₂, and NH₃) on the pristine and doped structures. We consider the substitutional doping occurring at the four distinct sites in the BC₆N lattice: the B, the N, and two distinct C sites. The formation energies of the doped structures indicate that they are stable. Upon Pt-doping, the BC₆N acquires a magnetization of $\sim 1 \mu_B$ for doping at the B and N sites, whereas systems doped at the two distinct C sites remain non-magnetic. The gaps of all doped systems change due to the Pt-doped states that are now located in the pristine gap. We also study the molecular adsorption properties of the doped structures using four gases: NO, NO₂, CO₂, and NH₃, where the gas molecule is placed close to the Pt atom. Adsorption of NO, NO₂, CO₂, and NH₃ is significantly enhanced on the doped structures. NO, NO₂, and NH₃ chemisorb with energies of ~ 1.3 – 3 eV, while CO₂ physisorb with ~ 0.7 eV. The interaction between the gas molecules and the doped sheets results in some charge transfer. This turns the doped systems non-magnetic for NO₂, CO₂, and NH₃, while it increases the magnetic moment for NO. The results of our study are important for applications of BC₆N, which include spintronics, gas filtration, and molecular sensing.

Supplementary Materials: The following supporting information can be downloaded at: <https://www.mdpi.com/article/10.3390/nano14090762/s1>, Figure S1: PDOS of NO₂ on the pristine system at different locations. Figure S2: PDOS of CO₂ on the pristine system at different locations. Figure S3: PDOS of NH₃ on the pristine system at different locations.

Author Contributions: Conceptualization, A.A.M.; data curation, N.M.A.; formal analysis, N.M.A. and H.M.A.-q.; investigation, N.M.A., M.M.F. and A.A.M.; methodology, A.A.M.; project administration, A.A.M.; resources, N.M.A., H.M.A.-q. and A.A.M.; software, N.M.A. and H.M.A.-q.; supervision, A.A.M.; validation, M.M.F.; visualization, N.M.A., M.M.F. and H.M.A.-q.; writing—original draft, N.M.A.; writing—review and editing, M.M.F., H.M.A.-q. and A.A.M. All authors have read and agreed to the published version of the manuscript.

Funding: This research received no external funding.

Data Availability Statement: The data presented in this study are available in article.

Acknowledgments: The authors would like to acknowledge the use of the resources of the Super-computing Laboratory at KAUST and the resources and technical services provided by the Scientific and High-Performance Computing Center at Imam Abdulrahman Bin Faisal University, Dammam, Saudi Arabia.

Conflicts of Interest: The authors declare no conflicts of interest.

References

1. Bhimanapati, G.R.; Lin, Z.; Meunier, V.; Jung, Y.; Cha, J.; Das, S.; Xiao, D.; Son, Y.; Strano, M.S.; Cooper, V.R.; et al. Recent advances in two-dimensional materials beyond graphene. *ACS Nano* **2015**, *9*, 11509–11539. [[CrossRef](#)] [[PubMed](#)]
2. Choi, W.; Lahiri, I.; Seelaboyina, R.; Kang, Y.S. Synthesis of graphene and its applications: A review. *Crit. Rev. Solid State Mater. Sci.* **2010**, *35*, 52–71. [[CrossRef](#)]
3. Li, X.; Zhu, H. Two-dimensional MoS₂: Properties, preparation, and applications. *J. Mater.* **2015**, *1*, 33–44. [[CrossRef](#)]
4. Manzeli, S.; Ovchinnikov, D.; Pasquier, D.; Yazyev, O.V.; Kis, A. 2D transition metal dichalcogenides. *Nat. Rev. Mater.* **2017**, *2*, 17033. [[CrossRef](#)]
5. Feng, J.W.; Liu, Y.J.; Wang, H.X.; Zhao, J.X.; Cai, Q.H.; Wang, X.Z. Gas adsorption on silicene: A theoretical study. *Comput. Mater. Sci.* **2014**, *87*, 218–226. [[CrossRef](#)]
6. Liu, Y.; Liu, W.; Hou, J.; Dai, Y.; Yang, J. Coronoid nanographene C₂₁₆ as hydrogen purification membrane: A density functional theory study. *Carbon* **2018**, *135*, 112–117. [[CrossRef](#)]
7. Kumar, R.; Sahoo, S.; Joanni, E.; Singh, R.K.; Yadav, R.M.; Verma, R.K.; Singh, D.P.; Tan, W.K.; Perez del Pino, A.; Moshkalev, S.A.; et al. A review on synthesis of graphene, h-BN and MoS₂ for energy storage applications: Recent progress and perspectives. *Nano Res.* **2019**, *12*, 2655–2694. [[CrossRef](#)]
8. Susarla, S.; Kutana, A.; Hachtel, J.A.; Kochat, V.; Apte, A.; Vajtai, R.; Idrobo, J.C.; Yakobson, B.I.; Tiwary, C.S.; Ajayan, P.M. Quaternary 2D transition metal dichalcogenides (TMDs) with tunable bandgap. *Adv. Mater.* **2017**, *29*, 1702457. [[CrossRef](#)] [[PubMed](#)]
9. Yang, Q.; Wang, Y.; Li, X.; Li, H.; Wang, Z.; Tang, Z.; Ma, L.; Mo, F.; Zhi, C. Recent Progress of MX ene-Based Nanomaterials in Flexible Energy Storage and Electronic Devices. *Energy Environ. Mater.* **2018**, *1*, 183–195. [[CrossRef](#)]
10. Salim, O.; Mahmoud, K.; Pant, K.; Joshi, R. Introduction to MXenes: Synthesis and characteristics. *Mater. Today Chem.* **2019**, *14*, 100191. [[CrossRef](#)]
11. Hong, Y.L.; Liu, Z.; Wang, L.; Zhou, T.; Ma, W.; Xu, C.; Feng, S.; Chen, L.; Chen, M.L.; Sun, D.M.; et al. Chemical vapor deposition of layered two-dimensional MoSi₂N₄ materials. *Science* **2020**, *369*, 670. [[CrossRef](#)] [[PubMed](#)]
12. Abbasi, A.; Sardroodi, J.J. The adsorption of sulfur trioxide and ozone molecules on stanene nanosheets investigated by DFT: Applications to gas sensor devices. *Phys. E Low-Dimens. Syst. Nanostruct.* **2019**, *108*, 382–390. [[CrossRef](#)]
13. Zhu, J.; Zhang, H.; Tong, Y.; Zhao, L.; Zhang, Y.; Qiu, Y.; Lin, X. First-principles investigations of metal (V, Nb, Ta)-doped monolayer MoS₂: Structural stability, electronic properties and adsorption of gas molecules. *Appl. Surf. Sci.* **2017**, *419*, 522–530. [[CrossRef](#)]
14. Yadav, S.; Tam, J.; Singh, C.V. A first principles study of hydrogen storage on lithium decorated two dimensional carbon allotropes. *Int. J. Hydrogen Energy* **2015**, *40*, 6128–6136. [[CrossRef](#)]
15. Fadlallah, M.M.; Abdelrahman, A.G.; Schwingenschlöggl, U.; Maarouf, A.A. Graphene and graphene nanomesh supported nickel clusters: Electronic, magnetic, and hydrogen storage properties. *Nanotechnology* **2019**, *30*, 085709. [[CrossRef](#)]
16. Donarelli, M.; Ottaviano, L. 2D materials for gas sensing applications: A review on graphene oxide, MoS₂, WS₂ and phosphorene. *Sensors* **2018**, *18*, 3638. [[CrossRef](#)]
17. Wang, B.; Gu, Y.; Chen, L.; Ji, L.; Zhu, H.; Sun, Q. Gas sensing devices based on two-dimensional materials: A review. *Nanotechnology* **2022**, *33*, 252001. [[CrossRef](#)]
18. Zhang, L.; Khan, K.; Zou, J.; Zhang, H.; Li, Y. Recent advances in emerging 2D material-based gas sensors: Potential in disease diagnosis. *Adv. Mater. Interfaces* **2019**, *6*, 1901329. [[CrossRef](#)]
19. Rahimi, R.; Solimannejad, M. Hydrogen storage on pristine and Li-decorated BC₆N monolayer from first-principles insights. *Mol. Phys.* **2021**, *119*, e1827177. [[CrossRef](#)]
20. Bafekry, A.; Naseri, M.; Fadlallah, M.M.; Abdolhosseini Sarsari, I.; Faraji, M.; Bagheri Khatibani, A.; Ghergherehchi, M.; Gogova, D. A novel two-dimensional boron–carbon–nitride (BCN) monolayer: A first-principles insight. *J. Appl. Phys.* **2021**, *130*, 114301. [[CrossRef](#)]
21. Lu, Y.; Yu, Y.; Zhu, X.; Wang, M. Two predicted two-dimensional BCN structures: A first-principles study. *Phys. E Low-Dimens. Syst. Nanostruct.* **2021**, *125*, 114413. [[CrossRef](#)]
22. Bafekry, A.; Stampfl, C. Band-gap control of graphenelike borocarbonitride g-BC₆N bilayers by electrical gating. *Phys. Rev. B* **2020**, *102*, 195411. [[CrossRef](#)]
23. Rani, P.; Jindal, V. Designing band gap of graphene by B and N dopant atoms. *RSC Adv.* **2013**, *3*, 802–812. [[CrossRef](#)]

24. Deng, X.; Wu, Y.; Dai, J.; Kang, D.; Zhang, D. Electronic structure tuning and band gap opening of graphene by hole/electron codoping. *Phys. Lett. A* **2011**, *375*, 3890–3894. [[CrossRef](#)]
25. Kouvetakis, J.; Sasaki, T.; Shen, C.; Hagiwara, R.; Lerner, M.; Krishnan, K.; Bartlett, N. Novel aspects of graphite intercalation by fluorine and fluorides and new B/C, C/N and B/C/N materials based on the graphite network. *Synth. Met.* **1989**, *34*, 1–7. [[CrossRef](#)]
26. Sadeghi, S.N.; Allaei, S.M.V.; Zebarjadi, M.; Esfarjani, K. Ultra-high lattice thermal conductivity and the effect of pressure in superhard hexagonal BC₂N. *J. Mater. Chem. C* **2020**, *8*, 15705–15716. [[CrossRef](#)]
27. Nehate, S.; Saikumar, A.; Prakash, A.; Sundaram, K. A review of boron carbon nitride thin films and progress in nanomaterials. *Mater. Today Adv.* **2020**, *8*, 100106. [[CrossRef](#)]
28. Wang, J.; Chen, C.; Yang, C.; Fan, Y.; Liu, D.; Lei, W. Boron carbon nitride (BCN) nanomaterials: Structures, synthesis and energy applications. *Curr. Graphene Sci.* **2018**, *2*, 3–14. [[CrossRef](#)]
29. Matsui, K.; Oda, S.; Yoshiura, K.; Nakajima, K.; Yasuda, N.; Hatakeyama, T. One-shot multiple borylation toward BN-doped nanographenes. *J. Am. Chem. Soc.* **2018**, *140*, 1195–1198. [[CrossRef](#)]
30. Aghaei, S.; Aasi, A.; Farhangdoust, S.; Panchapakesan, B. Graphene-like BC₆N nanosheets are potential candidates for detection of volatile organic compounds (VOCs) in human breath: A DFT study. *Appl. Surf. Sci.* **2021**, *536*, 147756. [[CrossRef](#)]
31. Bafekry, A. Graphene-like BC₆N single-layer: Tunable electronic and magnetic properties via thickness, gating, topological defects, and adatom/molecule. *Phys. E Low-Dimens. Syst. Nanostruct.* **2020**, *118*, 113850. [[CrossRef](#)]
32. Li, Y.; Gu, Q.; Johannessen, B.; Zheng, Z.; Li, C.; Luo, Y.; Zhang, Z.; Zhang, Q.; Fan, H.; Luo, W.; et al. Synergistic Pt doping and phase conversion engineering in two-dimensional MoS₂ for efficient hydrogen evolution. *Nano Energy* **2021**, *84*, 105898. [[CrossRef](#)]
33. Deng, J.; Li, H.; Xiao, J.; Tu, Y.; Deng, D.; Yang, H.; Tian, H.; Li, J.; Ren, P.; Bao, X. Triggering the electrocatalytic hydrogen evolution activity of the inert two-dimensional MoS₂ surface via single-atom metal doping. *Energy Environ. Sci.* **2015**, *8*, 1594–1601. [[CrossRef](#)]
34. Wang, X.; Zeng, F.; Qiu, H.; Guo, X.; Yao, Q.; Li, L.; Tang, J. Adsorption study of SF₆ molecules on Pt-doped two-dimensional material Ti₃C₂T_xMxene. *AIP Adv.* **2023**, *13*, 085217. [[CrossRef](#)]
35. Wu, P.; Huang, M. Investigation of adsorption behaviors, and electronic and magnetic properties for small gas molecules adsorbed on Pt-doped arsenene by density functional calculations. *RSC Adv.* **2023**, *13*, 3807–3817. [[CrossRef](#)]
36. Giannozzi, P.; Baroni, S.; Bonini, N.; Calandra, M.; Car, R.; Cavazzoni, C.; Ceresoli, D.; Chiarotti, G.L.; Cococcioni, M.; Dabo, I.; et al. QUANTUM ESPRESSO: A modular and open-source software project for quantum simulations of materials. *J. Phys. Condens. Matter* **2009**, *21*, 395502. [[CrossRef](#)]
37. Perdew, J.P.; Burke, K.; Ernzerhof, M. Generalized gradient approximation made simple. *Phys. Rev. Lett.* **1996**, *77*, 3865. [[CrossRef](#)]
38. Dion, M.; Rydberg, H.; Schröder, E.; Langreth, D.C.; Lundqvist, B.I. Van der Waals density functional for general geometries. *Phys. Rev. Lett.* **2004**, *92*, 246401. [[CrossRef](#)]
39. Aasi, A.; Mehdi Aghaei, S.; Panchapakesan, B. Outstanding performance of transition-metal-decorated single-layer graphene-like BC₆N nanosheets for disease biomarker detection in human breath. *ACS Omega* **2021**, *6*, 4696–4707. [[CrossRef](#)] [[PubMed](#)]
40. Babar, V.; Sharma, S.; Schwingenschlögl, U. Gas sensing performance of pristine and monovacant C₆BN monolayers evaluated by density functional theory and the nonequilibrium green's function formalism. *J. Phys. Chem. C* **2020**, *124*, 5853–5860. [[CrossRef](#)]
41. Degler, D.; Pereira de Carvalho, H.W.; Kvashnina, K.; Grunwaldt, J.D.; Weimar, U.; Barsan, N. Structure and chemistry of surface-doped Pt:SnO₂ gas sensing materials. *RSC Adv.* **2016**, *6*, 28149–28155. [[CrossRef](#)]
42. Ma, D.; Ju, W.; Li, T.; Zhang, X.; He, C.; Ma, B.; Lu, Z.; Yang, Z. The adsorption of CO and NO on the MoS₂ monolayer doped with Au, Pt, Pd, or Ni: A first-principles study. *Appl. Surf. Sci.* **2016**, *383*, 98–105. [[CrossRef](#)]
43. Ni, J.; Wang, W.; Quintana, M.; Jia, F.; Song, S. Adsorption of small gas molecules on strained monolayer WSe₂ doped with Pd, Ag, Au, and Pt: A computational investigation. *Appl. Surf. Sci.* **2020**, *514*, 145911. [[CrossRef](#)]
44. Cui, H.; Zhu, H.; Jia, P. Adsorption and sensing of SO₂ and SOF₂ molecule by Pt-doped HfSe₂ monolayer: A first-principles study. *Appl. Surf. Sci.* **2020**, *530*, 147242. [[CrossRef](#)]

Disclaimer/Publisher's Note: The statements, opinions and data contained in all publications are solely those of the individual author(s) and contributor(s) and not of MDPI and/or the editor(s). MDPI and/or the editor(s) disclaim responsibility for any injury to people or property resulting from any ideas, methods, instructions or products referred to in the content.